

LATEST DEVELOPMENTS FROM THE S-DALINAC*

W. Beinhauer, M. Brunken, H. Genz, M. Gopych, H.-D. Graef, T. Hartmann, M. Hertling, S. Khodyachykh, S. Kostial, U. Laier, O. Patalakha, M. Platz, A. Richter, B. Schweizer, A. Stascheck, O. Titze, S. Watzlawik, IKP, TU Darmstadt, Schlossgartenstr. 9, D-64289 Darmstadt.

Abstract

At the Darmstadt superconducting electron accelerator S-DALINAC the unloaded Q values of the accelerating cavities barely exceed $1 \cdot 10^9$. This is lower than the BCS limit by a factor of five and a factor of three lower than the design figure. In order to investigate this long known phenomenon systematically without interfering with accelerator operation, a vertical 2 K cryostat has been installed. Main subjects of the investigations are the influence of different surface preparation methods and the possibility of an insufficient magnetic shielding inside the accelerator cryostat. To improve the energy spread of the electron beam a DSP based hybrid (analog/digital) RF control system for the twelve cavities of the S-DALINAC is under development to replace the existing analog RF control system. Improved performance compared with the present system is expected mainly from using modern improved RF components and from applying feed forward corrections. In order to monitor the bremsstrahlung background caused by beam loss in the accelerator hall, so called Compton diodes have been designed. These photon detectors consist of aluminum, Plexiglas and lead. When they are hit by bremsstrahlung, an electric current (typically in the range of pA) proportional to the photon flux is generated between the aluminum and lead electrodes. Quantitative pictures of the transverse distribution of the electron beam are taken using optical transition radiation (OTR). The transverse phasespace is reconstructed using the filtered backprojection tomographic technique. Finally, beam parameters and the emittance are calculated statistically from the reconstructed distributions.

1 INTRODUCTION

Since 1987 the S-DALINAC [1] has provided more than 20000 hours of beamtime for a large variety of experiments. As a consequence, the beam parameters used for the different experiments cover a wide spectrum with electron energies between 2.5 MeV and 120 MeV, the beam currents vary from values as low as 1 nA up to 50 μ A (2.7 A peak current in FEL mode), with different time structures up to c.w. The design parameters of the accelerator are shown in table 1. Section 2 gives a short introduction into the layout of the S-DALINAC, Sect. 3 describes the properties of the superconducting cavities

*Work supported by DFG under contract number FOR 272/2-1 and through the 'Graduiertenkolleg Physik und Technik von Beschleunigern' under contract number GRK 410/2-01.

Table 1: Design parameters of the S-DALINAC.

Max. beam energy	130 MeV
Energyspread	$\pm 10^{-4}$
Max. current	20 μ A
Frequency	2.997 GHz
Duty cycle	c.w.

and covers the efforts that are currently undertaken to improve the Q values of the cavities, Sect. 4 deals with a planned replacement of the current analog RF control system by an analog/digital hybrid system in order to improve the beam quality and to enhance diagnostics. Sections 5 and 6 show new diagnostic tools developed at the S-DALINAC, such as a beam loss monitor using the Compton effect induced by bremsstrahlung and a tomographic technique relying on the signal of OTR targets to reconstruct the transversal phase space.

2 ACCELERATOR

The layout of the S-DALINAC, an S-Band recirculating linear electron accelerator with a maximum energy of 130 MeV, is shown in Fig. 1. The electrons are emitted thermionically from a cathode which is located inside a high voltage terminal at 250 keV.

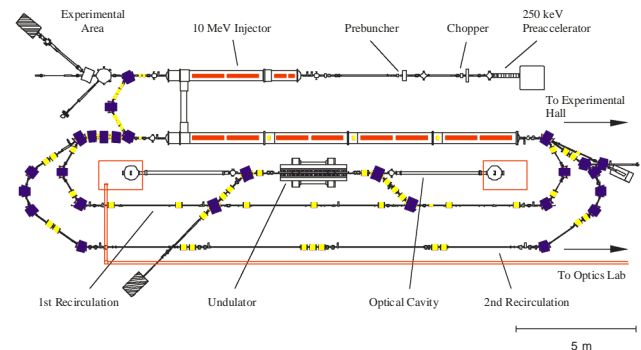


Figure 1: Layout of the S-DALINAC.

The electrostatically preaccelerated electron beam enters a chopper prebuncher section, where a time structure is imprinted onto the beam. The chopper and the prebuncher, normal conducting copper cavities, transform the D.C. beam emitted by the gun into 5 ps long electron bunches with a repetition rate of 3 GHz at the entrance of the superconducting injector linac. An additional

600 MHz subharmonic chopper/buncher section provides together with a pulsed electron emission a 10 MHz time structure, which is necessary for FEL operation. The injector linac consists of a two-cell capture cavity ($\beta=0.85$), followed by a five-cell cavity ($\beta=1$) and two 20-cell cavities. After the injector the electron beam with a maximum energy of 10 MeV may either be used for radiation physics experiments or for nuclear resonance fluorescence experiments or it can be bent by 180°, before being injected into the main accelerator. This superconducting linac has eight 20-cell cavities installed, which provide an energy gain of up to 40 MeV. After exiting from the linac the electron beam may be extracted towards the experimental hall or it can be reinjected twice into the main linac using two separated recirculating beam transport systems. After three passes the electron beam with an energy of up to 120 MeV and an energy spread of $\pm 3 \cdot 10^{-4}$ is delivered to the experimental hall, where it may be used for electron scattering experiments utilising a large spatial and momentum acceptance 180° spectrometer or a high resolution energy loss system with a 169° spectrometer. Additionally an infrared FEL with a 15 m long optical cavity, operating at wavelengths between 3 and 10 μm , is driven by the electron beam with a maximum energy of 50 MeV, which may be extracted from the first recirculation.

3 CAVITIES

The S-DALINAC uses eleven Niobium Cavities with a RRR of 300 that are operated at 2 K. The frequency of the accelerating π -mode is 3 GHz. Fig. 2 shows a picture of one of the 1 m long 20-cell resonators. The design value of the accelerating gradient, which is 5 MV/m is exceeded by almost all cavities, some resonators reach fields up to 10 MV/m. On the other hand, the design parameters assume a Q_0 of $3 \cdot 10^9$, which is 2/3 of the BCS limit, but unfortunately the highest Q value measured is slightly higher than $1 \cdot 10^9$.



Figure 2: Photograph of a 20-cell cavity.

This reduction in Q_0 increases the dissipated power per cavity at 5 MV/m from 4.2 W to 12.6 W. Currently the average Q_0 of all ten 20-cell cavities is $6.6 \cdot 10^8$. As a consequence the maximum beam energy of the S-DALINAC in c.w. mode is limited by the power of the installed helium refrigerator, which amounts only 120 W. Measurements of Q_0 as a function of temperature revealed that our cavities are limited by a residual resistance of at least 270 n Ω , compared to a BCS resistance of 50 n Ω at 2 K. The result is shown in Fig. 3.

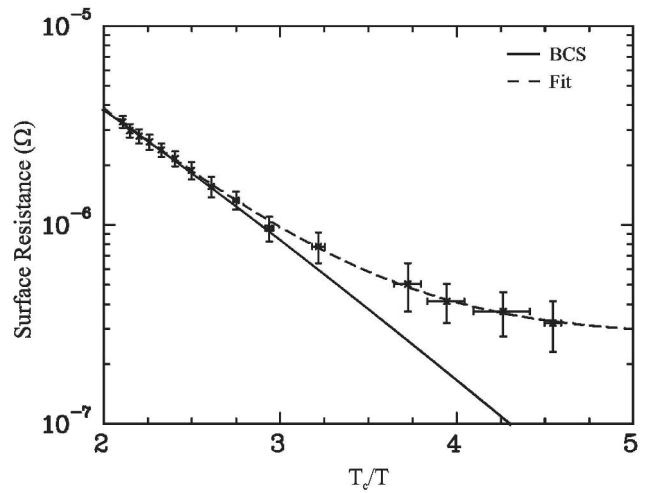


Figure 3: Surface Resistance as a function of the temperature. The dashed line shows a fit, the solid line represents the BCS resistance.

In order to understand the reason of this behaviour systematic tests using a vertical 2 K cryostat were performed. Different surface preparation methods were tested, such as a soft chemical polishing, which consists of an ultrasonic cleaning of the cavity with ultrapure water, oxidizing the inner surface with nitric acid (65% HNO_3) followed by rinsing with water. In a second step the niobium oxide is removed with hydrofluoric acid (40% HF); finally the cavity is rinsed and then dried by a nitrogen flow. By removing just a few atomic layers this method does not change the eigenfrequency of the cavity considerably. In another experiment 100 nm were removed, by substituting the oxidation with nitric acid by an anodization (40 V) in ammonium hydroxide (20% NH_4OH) which yields a much higher penetration depth of the oxide layer, that was also removed by hydrofluoric acid. Additionally cavities were heated up to 800 °C to remove hydrogen and there were also tests performed with a moderate heating of the cavity up to 120 °C for several days just prior to installation into the cryostat. Another field of interest was the development of a magnetic shielding for the cavities to study the influence of trapped magnetic flux. Inside the accelerator cryostat the situation is complicated by the fast tuner since it uses the magnetostretive effect. Additionally a nonuniform field distribution exists inside the helium vessel due to spots with increased magnetic field in the stainless steel walls of the vessel. These spots were induced during the forming process. A new magnetic shielding consisting of Cryoperm was designed and tested, both for the vertical cryostat and for the accelerator cryostat. Fig. 4 shows the effect of the new shielding on the magnetic field inside the accelerator cryostat.

Unfortunately none of the above measures have resulted in a Q_0 exceeding $1 \cdot 10^9$. In the future we plan to continue testing different preparation techniques and adapting them to the unfavourable geometry of a 20-cell 3 GHz cavity such as etching 100 μm of niobium from one of our cavities to ensure that the damage layer is completely

removed. Supplementary we try to enhance the magnetic shielding inside the accelerator cryostat to cope with possible magnetic field induced by the tuners.

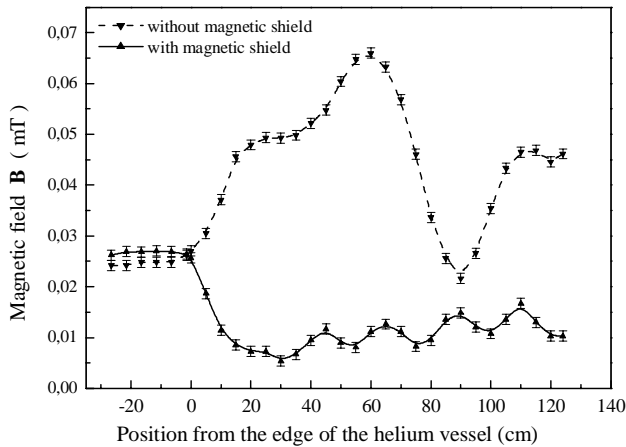


Figure 4: Magnetic field on the axis of the helium vessel inside the accelerator cryostat with and without shielding.

4 NEW RF CONTROL SYSTEM

The existing RF control at the S-DALINAC [2] uses down conversion into base band. The 3 GHz probe signals of the 12 superconducting cavities are converted down by a vector demodulator, that gives the two components of an RF vector in all four quadrants in the frame of the reference oscillator. The control itself is implemented as a self excited loop using proportional amplitude- and phase feedback circuits. The setpoints and gains for the control are currently set by an MC68020 processor, that also keeps track of the amplitude- and phase error signals. This control system has now worked for more than 12 years without major problems, but the energy spread achieved is still larger than specified in the design. For acceleration on crest the design figure is $\Delta E/E \leq \pm 10^{-4}$, whereas the present system achieves $\pm 10^{-3}$ under these conditions. Only by using non-isochronous recirculation an energy spread of $\Delta E/E = 3 \cdot 10^{-4}$ can be achieved. Therefore a new control system is developed to replace the existing one. Since the operational experience with the existing system is quite satisfactory, the conceptual design is adapted for the new control system, but more expense is paid on improving the energy spread. There will be two measures to reach a more accurate control: First the RF components used in the existing control system will be replaced by more accurate devices. The second measure is to use additional feed forward corrections. While the first replacements can be applied relatively easily, the application of feed forward corrections needs monitoring and diagnostics devices, which have the possibility to feed signals into the control loop. Long term monitoring is feasible with a digital system. Therefore all important RF signals will be digitized and fed to a DSP for diagnostic. In order to automate beam phase measurements, loaded Q determination etc., amplitude and phase of reflected

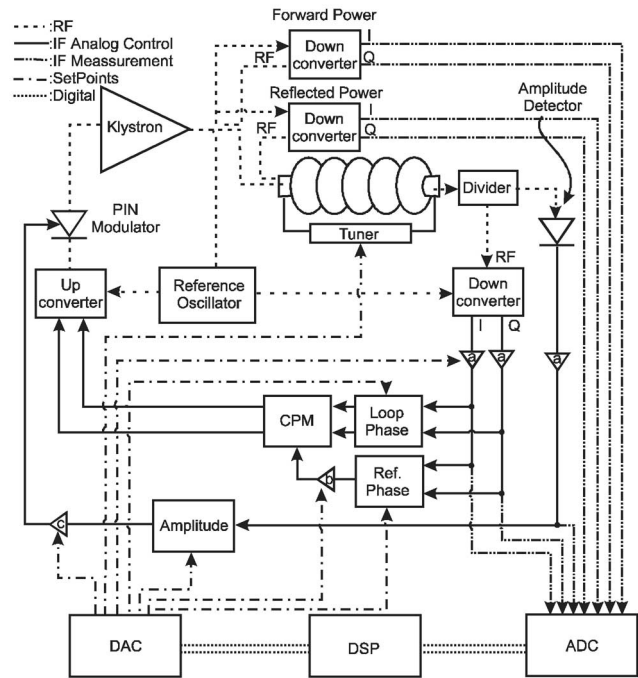


Figure 5: Block diagram of the new RF control system, where a represents the input gain, b the phase gain and c the amplitude gain.

power will be measured besides the cavity probe signal. Furthermore the electron gun will be controlled by the system. Setpoints and gains for the loop are set by the DSP, so that there is an interface for applying feed forward corrections calculated by the DSP. Since the cavity probe signal is measured by the existing control system, the RF boards have to be replaced by new designs to provide the additional RF signals. For a more accurate amplitude measurement an RF detector diode is used as in the existing control system, but by using a PIN diode as an amplitude modulator for the driver signal of the klystron (instead of low frequency multipliers as in the present system) there will be a separate amplitude control loop, which is independent of the quality of the used up- and down converters. To connect the DSP to the control loop, the intermediate frequency boards also need to be newly designed. By using a hybrid system, a maximum performance of the control loop is achieved, while still keeping the advantages (like feed forward capabilities) of a digital control system. Since the fast control is analog and additional errors like phase drifts are slow, the required conversion rate of the ADCs and DACs is in the range of a few 100 kHz. Therefore the implementation of the digital part will be easy compared to a pure digital RF control.

5 COMPTON DIODES

Since the S-DALINAC delivers electron beam for many different experiments, a large range of beam parameters is covered. To assist the operators in setting up the beam, a bremsstrahlung monitoring system for the accelerator vault has been developed. Requirements were

that the detector response should be linear with bremsstrahlung flux, and cheap and robust design was required so that a distributed monitoring system with minimal maintenance requirements could be established. The monitors used are so called Compton diodes [3]. They consist of an outer aluminum electrode, a Plexiglas insulation layer and an inner lead electrode. When a high energy photon impinges on the device, a large number of secondary electrons and photons are created in an electromagnetic cascade. The electrons created in a Compton process move preferably in forward direction (relative to the primary photon beam). The net electron current from the aluminum to the lead electrode can be used as a detector signal since it is directly proportional to the bremsstrahlung photon flux hitting the detector. The mechanical construction of such a Compton diode is shown in Fig. 6.

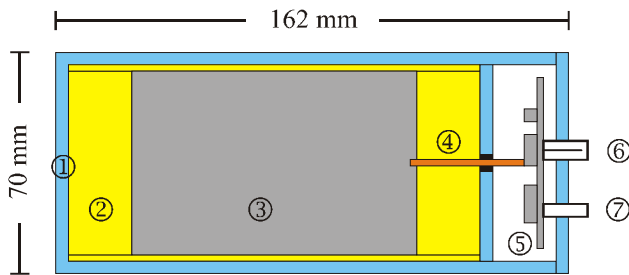


Figure 6: Layout of a Compton diode, 1 Aluminum electrode, 2 Plexiglas insulator, 3 Lead electrode, 4 Copper conductor, 5 Current-to-voltage converter, 6 Signal plug, 7 Power connector.

The outer aluminum shell is 4 mm thick, the Plexiglas insulation (front part) is 20 mm thick. This thickness is chosen such that the number of electrons in the electromagnetic cascade reaches its maximum value at the end of the Plexiglas layer. The lead electrode collects the electrons and also attenuates the photon flux. Therefore, no electron current at the rearside of the lead electrode counteracting the front current is generated. The lead also shields the current-to-voltage converter located at the back of the Compton diode from bremsstrahlung. The conversion factor of the circuit is 1 V of signal for 1 nA of Compton current induced in the detector. Calibration measurements were performed behind the injector and in the extraction section of the S-DALINAC. The detector signal versus the electron current on a 50 mm thick copper bremsstrahlung converter is displayed as black squares in Fig. 7.

The response to bremsstrahlung created with different electron energies was also measured. Numerical simulations of the Compton diode were performed with the Monte-Carlo code FLUKA. The aluminum, Plexiglas and lead volume was modelled. The creation of bremsstrahlung from electrons hitting a copper converter and the subsequent interactions of the photons with the detector was simulated. The electric charges flowing into and out of the lead electrode during the simulated

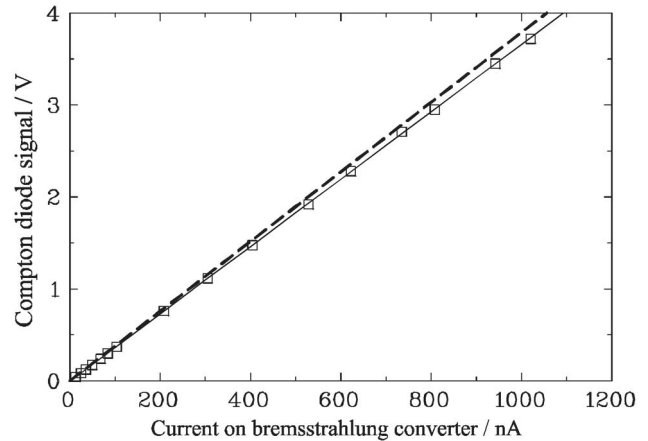


Figure 7: Compton diode signal in dependence of the beam current.

irradiation process are calculated by FLUKA and can be compared to the measured Compton current. For all experimental setups, the simulation results agree with the measurements to within $\pm 30\%$. The dashed line in Fig. 7 shows the simulation result for the experimental conditions. The response of the Compton diode to bremsstrahlung spectra with different endpoint energy were also simulated. It turns out that for endpoint energies between 10 and 130 MeV, the detector signal is approximately proportional to the photon number in the spectrum, independent of the endpoint energy. Because the Compton diodes are very simple to use, a number of further applications could be realized. A new beam line at the S-DALINAC (providing a photon beam) was taken into operation with a Compton diode directly located on the beam axis. Dark current measurements at the TTF linac at DESY, Hamburg were performed. The Compton diodes are presently under test as part of a machine interlock system for the new accelerator ELBE at Forschungszentrum Rossendorf.

6 TRANSVERSE PHASE SPACE TOMOGRAPHY

For diagnosis of the transverse beam parameters a set-up for imaging the transverse intensity distribution of the electron beam consisting of an optical transition radiation (OTR) target, a CCD camera and a PC with framegrabber card is used since a couple of years (see Fig. 8). The transverse emittance is calculated from a set of beam profiles measured with a quadrupole scan by a parabolic fit. The disadvantage of this method is that a gaussian distribution of the beam in phase space has to be assumed.

As an additional tool this set-up was expanded by a computer code written in the Interactive Data Language (IDL) [4] for reconstruction of the transverse phase space with a Filtered Backprojection algorithm. The advantage of this method is the capability of reconstructing the beam distribution in phase space without assuming any shape.

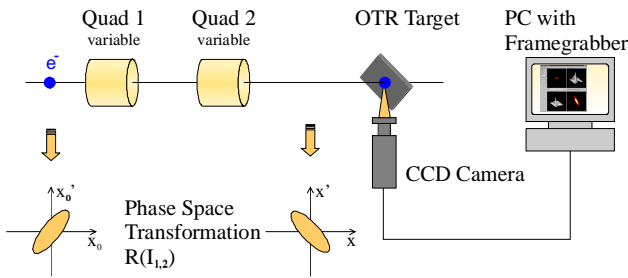


Figure 8: Set-up of the quadrupole scan with OTR target, CCD camera and digital processing.

The Filtered Backprojection algorithm we use to reconstruct the phase space is very sensitive on high frequency noise in the images. Therefore, all images have to be digitally processed before getting the projections for the reconstruction. Figure 9 illustrates the steps of the image processing: In the first step a background picture is subtracted to remove the offset and the effect of damaged pixels of the CCD camera. High signals on single pixels caused by x-rays from the beam passing the OTR target are removed by setting them to the mean value of the eight neighbouring values. Noise is reduced using a wavelet filter with hard thresholding, values smaller than 5% of the main peak are smoothed with a boxcar average of 21 pixels. Finally the contour is calculated where the main peak drops down to zero. The values outside the contour are set to zero.

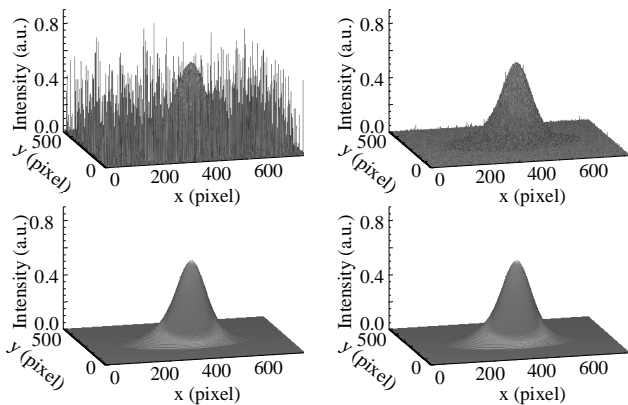


Figure 9: Processing of the OTR image: Underground subtraction (upper left), spot reduction (upper right), wavelet filter (lower left) and boxcar average (lower right).

The accuracy of the Filtered Backprojection algorithm was properly investigated. In simulations with 18 projections interpolated to 90 projections an unsymmetrical phase space distribution could be reconstructed with an emittance error of less than 15%. First measurements at the injector linac of the S-DALINAC at an energy of 8 MeV showed good agreement of the emittance with respect to the common method. Figure 10 shows the reconstruction of the horizontal phase space distribution with an emittance of $\epsilon_n = 2.14 \pi \text{ mm mrad}$.

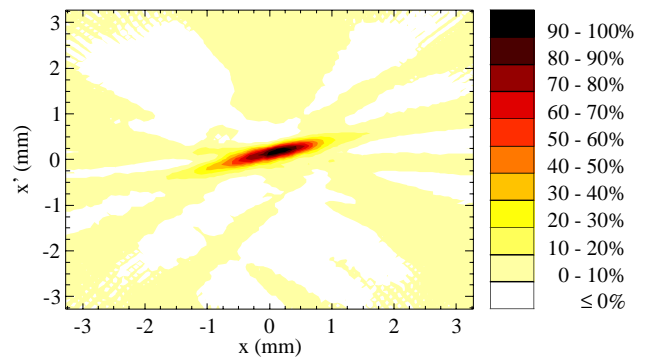


Figure 10: Reconstruction of the horizontal phase space.

7 SUMMARY

Further studies concerning both different cavity preparation methods and improvements of the magnetic shielding will be made. The development of a new RF control system is currently performed aiming at a reduction of the energyspread. To improve the beam quality of the S-DALINAC two diagnostic tools were developed. A set of robust bremsstrahlungs monitors was installed to observe beam losses. Finally a new measurement tool was implemented which allows a reconstruction of transversal phase space using tomographic techniques.

REFERENCES

- [1] A. Richter, Proc. 5th Europ. Part. Acc. Conf., Eds. S. Myers, A. Pacheco, R. Pasucal, Ch. Petit-Jean-Genaz and J. Poole, Sitges (Barcelona), (1996) 110.
- [2] H.-D. Graef and A. Richter, Proc. Lin. Acc. Conf., Newport News, (1988) 231.
- [3] B. Gross, Compton Diodes, Zeitschrift fuer angewandte Physik, (1970) Bd. 30, Heft 5, 323.
- [4] Research Systems, Inc., *The Interactive Data Language*, Version 5.0.